Study on Effect of Duration of the Ultrasonication Process on Solvent-free Polyurethane/Organoclay Nanocomposite Coatings: Structural Characteristics and Barrier Performance Analysis

M. Heidarian, M. R. Shishesaz

Technical Inspection Engineering Department, Petroleum University of Technology, Abadan, Iran

Received 3 July 2010; accepted 1 January 2011
DOI 10.1002/app.34077
Published online in Wiley Online Library (wileyonlinelibrary.com).

ABSTRACT: In this study, effect of duration of ultrasonication process on structural characteristics and barrier properties of solvent-free castor oil-based polyurethane (PU)/organically modified montmorillonite (OMMT) nanocomposites was investigated. A series of PU/OMMT composites were synthesized by *in situ* polymerization technique through an ultrasonication-assisted process at various processing durations. Effect of ultrasonication duration on de-agglomeration of clay stacks in castor oil dispersions was evaluated by optical microscopy, sedimentation test, and viscosity measurement. Wide angle X-ray diffraction and Fourier-transform infrared spectroscopy were employed to investigate the effect of processing time on degree of delamination of clay platelets and interfacial strength between clay layers and PU matrix. Also, surface morphology of the nanocomposites was analyzed by atomic force microscopy. The results showed that by increasing the ultrasonication time up to 60 min, the size of clay agglomerates decreased and the interlayer spacing of clay platelets increased. To evaluate the effect of ultrasonication duration on transport properties of the PU/OMMT composites, diffusion coefficient and permeability were determined through water uptake test. Electrochemical impedance spectroscopy was carried out to analyze the barrier properties and to evaluate the corrosion performance of these composite coatings on carbon steel panels. It was found that by increasing sonication time, the barrier property of nanocomposites against diffusion of water molecules improved, which is due to further separation of clay platelets, enhancement of the traveling pathways for water molecules and improvement of interactions between the two components. J Appl Polym Sci 000: 000–000, 2012

Key words: nanocomposite; barrier; coatings; wide angle X-ray diffraction; atomic force microscopy

INTRODUCTION

Polymer clay nanocomposites have attracted a great deal of research interest in recent years, because they exhibit greatly enhanced properties compared with conventional microcomposites and pure polymers.[1–6] The excellent barrier properties with intensively reduced permeability of gases, water, and hydrocarbons are one of the most attractive and useful properties of these nanocomposites in coating, packaging, and membrane applications.[7–9]

The efficiency of the clay to modify the barrier properties of the polymer is directly related to the aspect ratio, dispersion of clay layers in polymer, and strength of interfacial interactions between the polymeric matrix and clay platelets.[10–13] Increasing the extent of exfoliation (delamination of clay layers) plays an important role in terms of providing barrier properties for the nanocomposite polymeric systems without drawbacks of conventional microcomposites including weight increase, brittleness, and opacity loss,[14] which in turn leads to lower diffusivity of surrounding environment. This may be attributed to enhanced tortuosity of the diffusion pathway in the matrix[7] and enhanced restricted segmental motion of the polymer chains within the clay gallery spaces and at the interface with the clay layers.[15] On the other hand, poor dispersion of nanoparticles leads to inferior barrier property of the system.[16] Relationship between the degree of delamination of clay layers and extent of improvement in barrier properties is such that some researchers have worked to build diffusivity models from the water uptake behavior of polymer clay nanocomposites to determine the degree of exfoliation of clay layers by using diffusivity measurements.[17]

Despite lots of researches that have been devoted to this class of materials in the past two

Correspondence to: M. Heidarian (mortezaheidarian@yahoo.com).

Contract grant sponsors: Research and Development Centre of Bandar Imam Petrochemical Complex, Bajak Paint Co. Ltd.

decades, the current commercial applications of polymer clay nanocomposites are limited due to inherent incompatibility between clay layers and polymers and lack of consistent processing methods for de-agglomeration and delamination of clay stacks.[18,19] Clay stacks tend to aggregate together during mixing with polymer matrix due to extensive surface area and cohesive forces between them which hinder the formation of a delaminated nanocomposite structure.[20] However, it is assumed that breaking down of clay aggregates and delamination of clay layers can be achieved through a proper combination of mechanical forces such as shear or impact and diffusion of the small molecules into space between clay sheets.[21,22] Considering that the chemical compatibility between natural clay and polymeric matrix can be obtained by modification of clay with intercalating surfactants for better diffusion of polymer chains, the processing conditions must be optimized to give clay tactoids that are minimized in size and to force the monomers to diffuse further between clay layers.[23] Researchers have used several processing methods for dispersing and delaminating nanoclay layers including mechanical agitation, shear mixing, high pressure mixing, noncontact mixing and ultrasonic vibration.[20] Among the aforementioned techniques, there are lots of reports, which indicate that ultrasonication is an effective method to improve dispersion and delamination of clay layers[20,24] and also to reduce air bubbles at the interface between clay platelets and resin molecules.[25]

To understand the effect of sonication processing parameters on dispersion of clay tactoids, and thus the resulted properties of polymer clay nanocomposites, further investigations in the case of role of time, temperature, and ultrasonic wave amplitude are still required. Lam et al.[26] have recently reported a study on the effect of ultrasonication time on dispersion of nanoclay clusters in an epoxy composite. It was found that nanoclay cluster sizes altered by changing the sonication times without any variation in interplanar distance of the clay layers. It was also reported that there exist an optimum ultrasonication time to achieve minimum cluster size. Also, Wang and Qin[27] indicated that the clay layers were found to be separated further in epoxy–nanoclay composite with an increase in the ultrasonic stirring duration.

To our best knowledge, there is not any available report that fully explores the effect of ultrasonication time on the structural characteristics and transport properties of polymer clay nanocomposites, especially in case of solvent-free PU-based nanocomposites. In this study, 3 wt % PU/OMMT composites were synthesized by *in situ* polymerization method through a sonication assisted technique at various processing durations. Optical microscopy, sedimentation test, viscosity measurement, wide angle X-ray diffraction (WAXD), Fourier-transform infrared spectroscopy (FTIR), and atomic force microscopy (AFM) techniques were employed to characterize the structure of castor oil/OMMT dispersions and PU/OMMT nanocomposites. The diffusion coefficients and the maximum water uptake of the 3 wt % PU/OMMT composite films were measured by water uptake test. Also, to study the barrier properties and to evaluate the corrosion performance of these composites as protective organic coatings on carbon steel panels, electrochemical impedance spectroscopy (EIS) was performed. From the experimental results, the correlation between the structural characteristics of the synthesized composites and the resulted transport properties is discussed.

EXPERIMENTAL

Materials

A commercial grade castor oil (Albodur 912 VP; OH_v = 210 mg KOH/g, average functionality = 2.3) was purchased from Alberdingk Boley Co. It was dehydrated at 50°C in vacuum. Polymeric methylenediphenylenediisocyanate (P-MDI; Suprasec 2496; NCO wt % = 31.3, average functionality = 2.5; Huntsman PUs) was dried for 1 h in vacuum oven to remove any trace of moisture. Modified montmorillonite clay (Cloisite 30B) was received from Southern Clay Products with methyl, tallow, bis-2-hydroxyethyl, quaternary ammonium as modifier, and it was dehumidified at 80°C for 24 h.

Synthesis of PU nanocomposites

Nanocomposites were synthesized by *in situ* polymerization in presence of clay. Three weight percent of Cloisite 30B (C30B) was first dispersed in dehydrated castor oil using propeller stirrer at 1200 rpm for 2 h at 70°C in a plastic flask (with nitrogen inlet and temperature control jacket). This was followed by sonication process of different durations, namely, 15, 30, and 60 min at 60°C with an external cooling bath (It is worth mentioning that based on a series of preliminary experiments, the specified amount of clay is selected from a wide variety of clay loadings between 1 and 5 wt % for more thorough investigations in the case of effect of processing conditions on the PU/clay nanocomposites by considering the practical application and performance of the resulted material). The ultrasonication process was performed at a frequency of 20 kHz with an inlet ultrasound power of around 1 W/mL (UIP 1000hd ultrasonic processor; titanium sonotrode with 18-mm tip

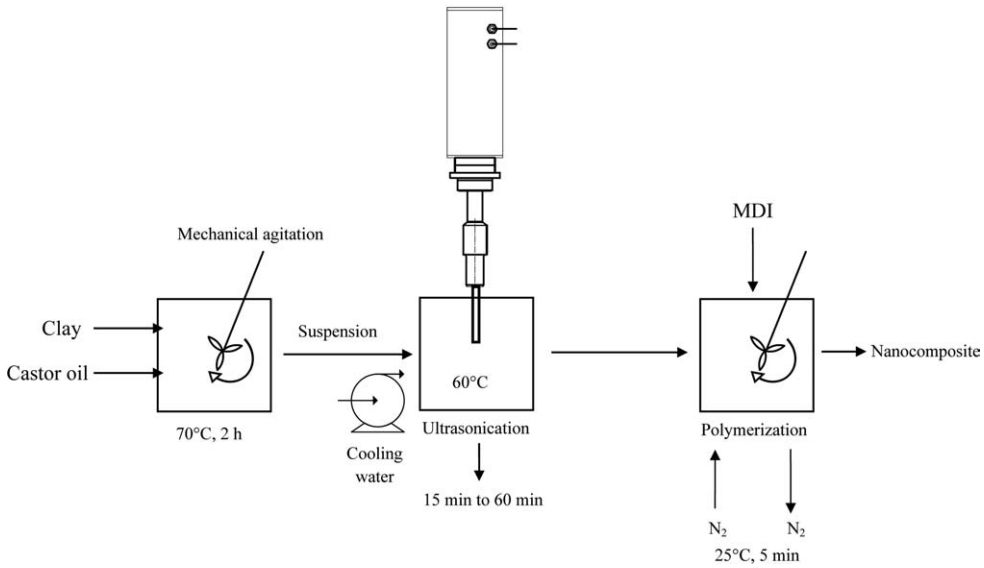

Figure 1 Schematic illustration of PU clay nanocomposite preparation under various processing conditions.

diameter; Hielscher ultrasound technology). The mixture then reacted with P-MDI with continuous stirring under nitrogen atmosphere while the NCO:OH ratio was kept at 1. The blends were then degassed under vacuum and immediately poured into molds. Samples were allowed to cure for 2 weeks at 60°C. As schematically depicted in Figure 1, four sets of composites containing 3 wt % filler on solid content of the system were prepared under different premixing conditions, namely, 2-h mechanical agitation and 15-, 30-, and 60-min sonication (note that premixing means mixing the clay with polyol without hardener).

Structural characterization of nanocomposites

The optical homogeneity of the polyol/clay dispersions and effect of sonication process on de-agglomeration of clay aggregates were examined using a BX-50 Olympus optical microscope. Also, the suspension stability was analyzed by a sedimentation method. For this purpose, the blends were kept motionlessly at 50°C for 2 weeks to observe the amounts of clay precipitation and phase separation. The viscosity of castor oil/OMMT suspensions was determined using a REL multispeed digital viscometer equipped with cone/plate geometry (diameter: 20 mm; angle: 0.5°) at a constant speed of 185 rpm and 30°C. The maximum deviation for viscosity results was 2%.

WAXD of nanocomposite films was conducted by subjecting the films to X-ray radiation at room temperature. The films were analyzed using a X'PERT Philips diffractometer system. The radiation was CuKα ($\lambda = 1.54$ Å) at 40 KV and 40 mA. Diffraction was performed from $2\theta = 1°$–$10°$ at a scanning rate of 0.5°/min with a step size 0.02°.

To monitor the interfacial reactions between organoclay platelets and PU and to understand the effect of clay layers on hydrogen bond formation in PU matrix, pristine PU, pure OMMT, and PU/OMMT composites, prepared by different premixing conditions, were characterized by FTIR. Infrared spectra were conducted on an Equinox 55 FTIR (Bruker, Germany) using KBr disk technique, with a wave number resolution of 4 cm^{-1} within the range of 400–4000 cm^{-1}.

Surface morphology of nanocomposites

The surface morphology of the pure PU and 3 wt % PU/OMMT nanocomposites, premixed by 15-, 30-, and 60-min sonication, was determined by AFM. Measurements were performed under ambient conditions using a commercial atomic force microscope (Nanosurf easyScan 2 AFM, Switzerland). The contact-mode AFM technique was used for all images. An area of 30 micron was scanned at a constant force with set point of 20 nN. The roughness analysis was performed on the dimensions of 30×30 μm^2. The root-mean-square (Rms) roughness value is the standard deviation of the Z (height) values calculated within the given area as:

$$\mathrm{Rms} = \sqrt{\frac{\sum (Z_i - Z_{\mathrm{ave}})^2}{N}} \quad (1)$$

where Z_i is the current Z value, and Z_{ave} is the average of the Z values, and N is the number of data points with the given area.[28] All the mean roughness

values were obtained by averaging the results from three AFM images.

Moisture absorption measurement

Water absorption measurement was carried out according to the specification, ASTM D 570-98. The molded samples, prepared by different processing conditions (as described before), were cut into the form of discs 5 cm in diameter and 3.2 mm in thickness. The discs were washed with acetone, dried completely, and the initial weights were measured. The specimens were then immersed in distilled water at 25 ± 2°C. At predetermined intervals, specimens were taken out of water and were weighed on an analytical balance with a resolution of 0.1 mg. All the measurements were obtained from at least three experiments to ensure reproducibility. The moisture uptake at any point of time was determined using the following equation:

$$M_t(\text{wt \%}) = \left[\frac{W_t - W_0}{W_0}\right] \times 100, \tag{2}$$

where M_t, W_t, and W_0 are the moisture content at a given time, instantaneous, and initial weights of the samples, respectively.

The mechanism of moisture diffusion in polymers has been extensively studied.[16,25] Moisture diffusion in polymer composites at low temperatures can be estimated by the Fick's second law with a constant diffusivity, D, which describes the nonsteady state diffusion of a substance and is given by[17]:

$$\frac{M_t}{M_\infty} = 1 - \frac{8}{\pi^2}\sum\nolimits_{n=0}^{\infty} \frac{1}{(2n+1)^2} \exp\left[-\left(\frac{D(2n+1)^2 t}{h^2}\right)\pi^2\right] \tag{3}$$

where M_t and M_∞ are the moisture contents at time t and at equilibrium, respectively. D is the diffusion coefficient and h is the sample thickness. At the initial stages of diffusion, eq. (3) can be approximated by:

$$\frac{M_t}{M_\infty} = \frac{4}{h}\left(\frac{Dt}{\pi}\right)^{1/2} \tag{4}$$

Hence from the Fick's second law, diffusivity (D) can be determined from the initial slope of the curve plotted for the percentage water uptake, M_t, versus the square root of time, $t^{1/2}$.

Sorption coefficient (S) is a thermodynamic parameter which depends on the strength of the interactions in the polymer/penetrant mixture. Sorption describes the initial penetration and dispersal of penetrant molecules into the polymer matrix. It is calculated from the equilibrium swelling using the following equation[29]:

$$S = \frac{m_\infty}{m_p}, \tag{5}$$

where m_∞ represents mass of the solvent taken up at the equilibrium and m_p represents initial mass of the sample. Permeability (P) is a combination of sorption and diffusion processes and hence the permeability of solvent molecules into polymer membrane depends upon both diffusivity and sorptivity. P can be determined from the following empirical relation[29,30]:

$$P = D \times S, \tag{6}$$

Electrochemical measurement of water uptake

Coatings protect the substrate in many ways, including preventing damaging species access to the substrate. One of the ubiquitous natural molecules that damage the substrate is water. Substrate degradation depends on the water concentration and ion transport at the interface and flux towards the substrate. The protection efficiency is inversely related to the corrosive species diffusion.[31,32] One of the methods commonly used to study coatings performance is EIS. Penetration of water molecules into the polymer structure changes the coating resistance and capacitance which in turn influence the impedance response of the metal/coating system under the application of alternating potential signal. During the initial stage of coating exposure, the volumetric percentage of water uptake also can be estimated by Brasher–Kingsbury empirical equation[33]:

$$X_v = \frac{\log\left(C_1/C_0\right)}{\log 80} \times 100\%, \tag{7}$$

where C_1 and C_0 are the measured capacitances at times t_1 and t_0, respectively. Thus, from the plots of the impedance diagrams versus exposure time in an aggressive solution, the amount of water uptake and corrosion protection afforded by organic coatings can be determined.

For preparation of coated panels, 3 wt % PU/OMMT composites, prepared by different processing conditions, were applied on steel substrates with a film applicator before curing. Cold rolled carbon steel panels (6.5 × 6.5 × 0.3 cm^3) were used as metallic substrates. The panels were subjected to a sequence of a chemical cleaning and a mechanical surface polishing to remove any trace of surface oxides. Before coating application, the panels were extensively cleaned with acetone and

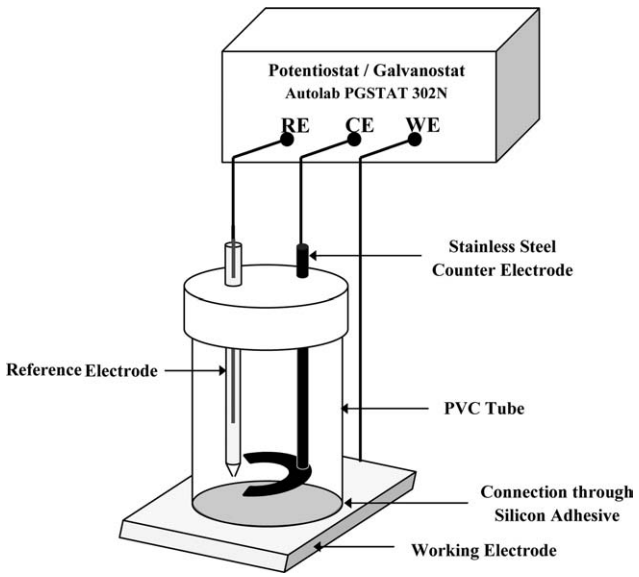

Figure 2 Schematic illustration of the electrochemical cell.

toluene. The thickness of dry coatings was measured with Elcometer FN 465[3] digital coating thickness meter (Elcometer Co. Ltd.) and was chosen in the range 50–60 μm.

To determine electrochemical impedance response of the coated panels, A PVC tube of 4.7-cm inner diameter was pasted with silicon adhesive on surface of coated substrates. The electrochemical cell was prepared by placing the aforementioned samples horizontally at the bottom in a standard flat cell configuration. The exposed sample surface area of 17 cm^2 acted as the working electrode. A large area stainless steel counter electrode was positioned parallel to the exposed sample and a saturated Ag|AgCl electrode was employed as the reference electrode. Schematic illustration of the electrochemical cell is shown in Figure 2.

The EIS measurements were carried out with Autolab PGSTAT 302*N* Potentiosat/Galvanostat and FRA2 frequency response analyzer at open circuit potential with AC amplitude of 20 mV over a frequency ranging from 100 kHz to 1 mHz. The samples were submitted to a total immersion in 5 wt % aerated NaCl aqueous solution. The impedance diagrams were obtained at different exposure times up to 30 days. Interpretation of impedance data was performed using Autolab Frequency Response Analyzer (FRA) software.

RESULTS AND DISCUSSION

Dispersion of organoclay in castor oil

Figure 3 presents the optical micrographs of castor oil/OMMT suspensions prepared after 2-h mechanical agitation, followed by sonication of various durations, including 15, 30 and 60 min. The castor oil/OMMT dispersion, prepared after 2-h mechanical agitation, contained large amounts of agglomerates of clay stacks [shown in Fig. 3(a)]. These agglomerates are formed during wetting of OMMT with castor oil due to large surface area of nanoclay and cohesive forces between clay stacks. By application of sonication process and increasing its duration, as shown in Figure 3(b–d), the size of clay agglomerates is reduced, and their distribution in castor oil matrix is improved. As mentioned earlier, the processing condition must be capable of providing enough mechanical forces to significantly break-up the agglomerates and to force the polymer chains to diffuse between clay layers. While the sonication process is applied, the cavitation shockwaves combined with extreme temperature gradients results in high velocity collisions between clay aggregates and accelerated molecular diffusion of castor oil, which leads to significant break-up of clay agglomerates. These effects are enhanced as the duration of sonication is increased. As shown in Figure 3(d), after 60-min sonication, almost all of the clay agglomerates had completely disappeared. The remaining agglomerates could be attributed to impurities or unmodified clay in commercial products.

Stability of suspensions

Figure 4 shows the suspension state of castor oil/OMMT mixtures, prepared after 2-h mechanical agitation and 15-, 30-, and 60-min sonication. Suspensions were placed at 50°C for 2 weeks after preparation. In case of mechanically agitated dispersion, extensive phase separation and sediment was observed and OMMT precipitation was initiated right after stopping stirring [shown in Fig. 4(a)]. As it was illustrated by optical microscopy, there were lots of large agglomerates in this suspension due to insufficient shear and impact forces and low mobility of castor oil molecules, resulted from mechanical agitation. So, castor oil molecules cannot penetrate into these agglomerates to diffuse between layers of clay stacks. Therefore, clay agglomerates precipitate due to the gravity during the sedimentation test. However, after 15-min sonication, the extent of phase separation was decreased greatly. Also, after 30- and 60-min sonication, there is no significant phase separation and sediment. As a result of sonication, significant beak-up of the clay aggregates takes place due to extreme motions such as shearing or collision against each other. Therefore, the size of aggregates and clay stacks reduces. This in turn causes that castor oil molecules diffuse further into the space between clay layers. By separation of clay platelets, interactions between clay and polymeric matrix increase which in turn improve suspension

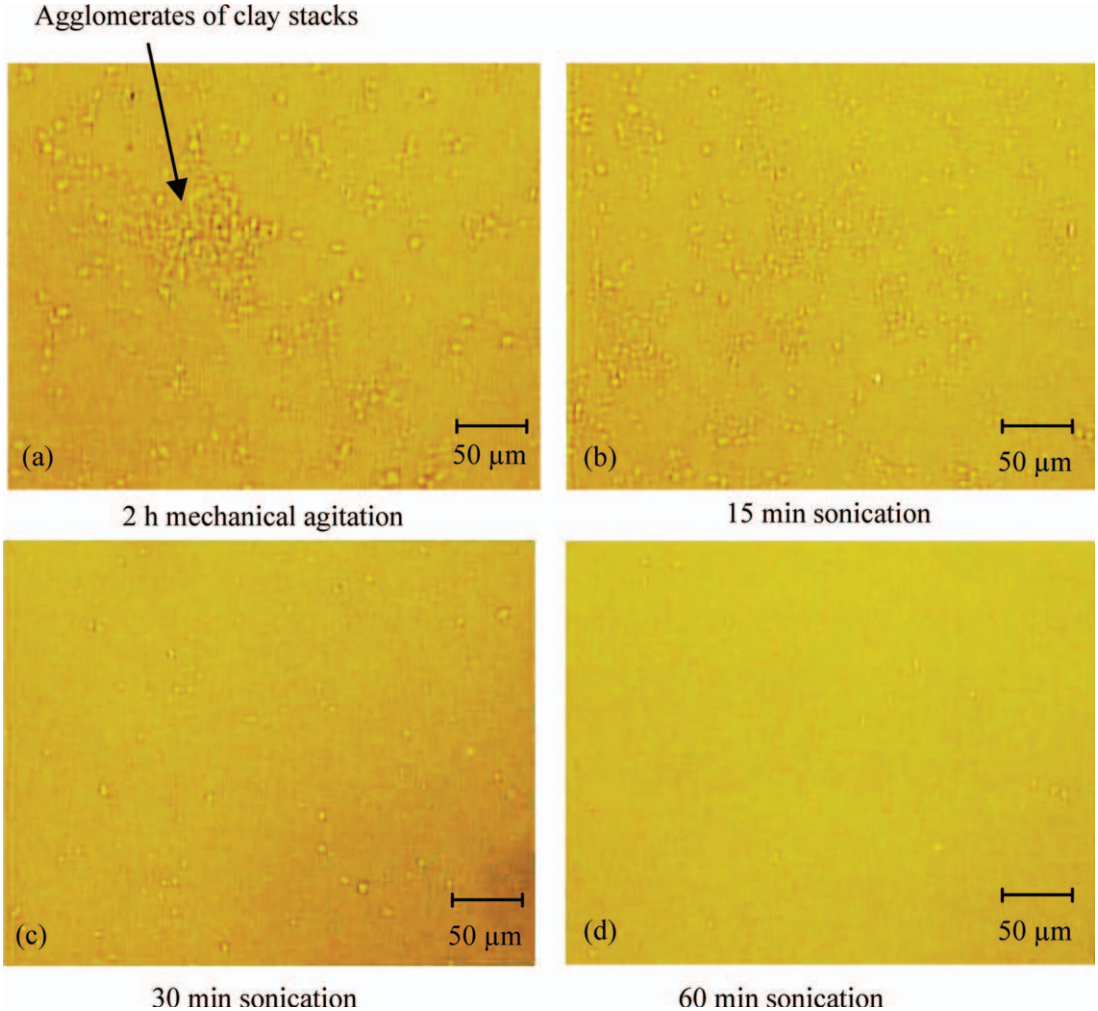

Figure 3 Optical micrographs of 3 wt % organoclay/castor oil suspensions: (a) after 2-h mechanical agitation, (b) after 15-min sonication, (c) after 30-min sonication, and (d) after 60-min sonication. [Color figure can be viewed in the online issue, which is available at wileyonlinelibrary.com.]

stability. Also, due to improvement of clay interlayer spacing, the organifier on OMMT surface could be further dissolved in castor oil and could act as the surfactant between layered silicate and castor oil. Hence, stable suspensions of OMMT in castor oil could be formed.

Viscosity

Rheological responses of polymer/clay dispersions offer suitable insights into their microstructure[34] and could be used to quantify the global average of the degree of intercalation/exfoliation/dispersion of clay stacks across the whole test specimen.

The viscosity values of 3 wt % castor oil/OMMT dispersions, prepared by different processing conditions, are shown in Figure 5. The pristine castor oil shows a viscosity of 408 mPa s. As shown in Figure 5, only a slight increase in viscosity was observed after mixing OMMT with castor oil by mechanical agitation for 2 h. However, by application of sonication process and increasing its duration, a significant increase in viscosity was resulted and the dispersion, prepared by 60-min sonication, represents almost a threefold increase of the viscosity with respect to the neat castor oil.

Viscosity is a measure of internal friction of the dispersion when sheared. As aforementioned, ultrasonication in castor oil/OMMT dispersions leads to size reduction of clay agglomerates and enhancement of particle number per unit volume, better dispersion and higher aspect ratio of clay stacks and improved penetration of castor oil molecules between clay sheets. These in turn increase frictional interactions between silicate layers. By further intercalation of castor oil chains, van der Walls forces between clay layers and castor oil molecules are strengthened as well. Also, further H-bonding between hydroxyl groups on clay surface (clay structural OH groups and organifier OH groups) and

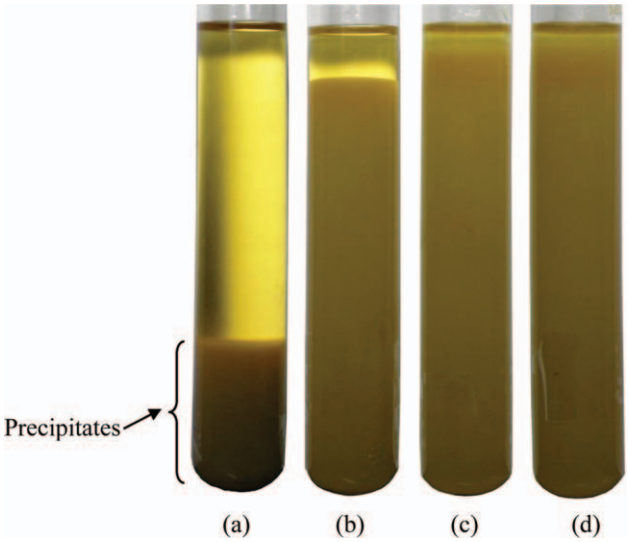

Figure 4 Suspension state of 3 wt % organoclay/castor oil dispersions: (a) after 2-h mechanical agitation, (b) after 15-min sonication, (c) after 30-min sonication, and (d) after 60-min sonication. [Color figure can be viewed in the online issue, which is available at wileyonlinelibrary.com.]

carbonyl groups of castor oil may be established which in turn results in improved frictional forces and viscosity. Some researchers also reported that the significant enhancement of viscosity is arisen from the formation of face-edge and edge-edge house-card structure.[36,37]

X-ray diffraction analysis

The *d*-spacing of OMMT organoclay in PU clay composites, prepared through different premixing conditions, was examined by X-ray diffraction. The results are presented in Figure 6 and Table I. Pure OMMT displays a peak at $2\theta = 4.78^\circ$, which corresponds to d_{001} basal spacing of 18.48 Å. In the case of 3 wt % PU/OMMT composite, premixed for 2 h by mechanical agitation, this peak shifts to $2\theta = 3.21^\circ$, which indicates a little expansion of the basal spacing due to low penetration of the PU chains within the gallery spaces. By using 15- and 30-min sonication at premixing step, not only the peak position was shifted to lower angles ($2\theta = 2.53^\circ$ and $2\theta = 2.37^\circ$, respectively) but also a decrease in peak intensity was observed. This suggests that a partial exfoliation of OMMT in PU matrix has taken place. When the mixture was proceed with 60-min sonication, the peak on WAXD curve had almost disappeared, which suggested the exfoliation of silicate layers or much too large spacing between the layers.

By applying sonication and increasing its duration at the premixing step, significant break-up of clay agglomerates and penetration of castor oil molecules between clay sheets take place which in turn increase the basal spacing of silicate layers. Because of this, P-MDI have more chance to diffuse into galleries during polymerization step to further promote interagallery reactions with OH groups of clay organifier and castor oil molecules which diffused there at premixing step. This in turn leads to larger expansion of OMMT gallery spacing.

Fourier-transform infrared spectroscopy

To monitor the effect of ultrasonication stirring time on chemical structure of PU in composites and interfacial hydrogen bond formation between clay layers and PU matrix, the FTIR spectra of OMMT, pristine PU, and 3 wt % PU/OMMT composites premixed during 2-h mechanical agitation and 15-, 30-, and 60-min sonication were measured as shown in Figure 7.

The FTIR spectra of OMMT clay is presented in Figure 7(a). The structural —OH stretching peak

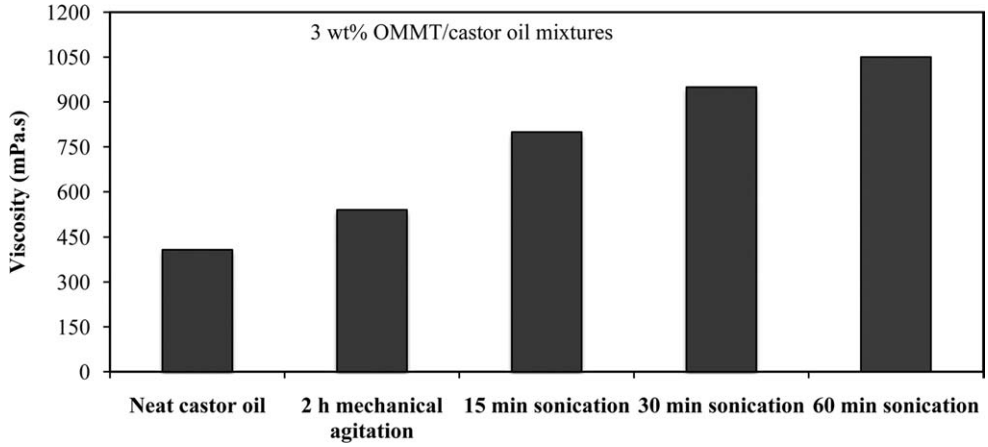

Figure 5 Viscosity of castor oil/OMMT dispersions containing 3 wt % OMMT prepared under different premixing conditions.

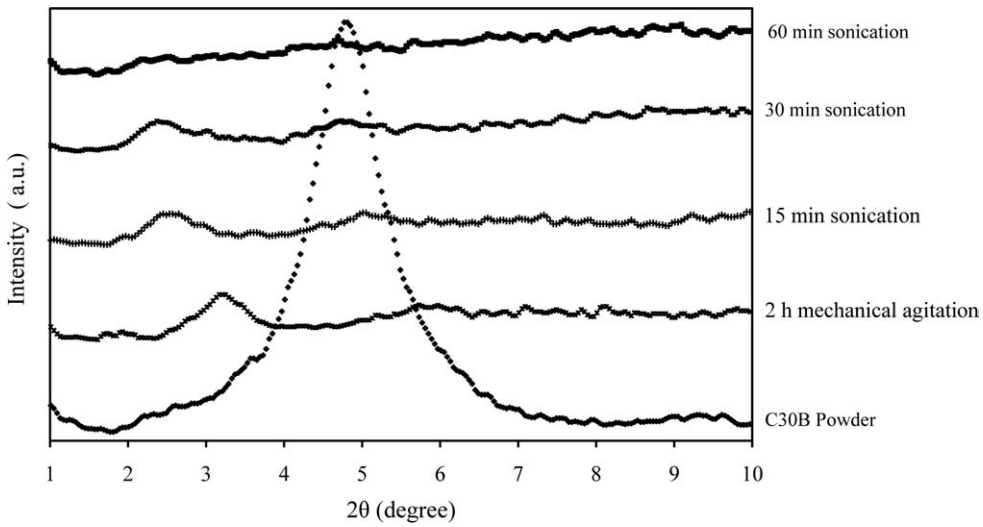

Figure 6 WAXD of pure C30B and 3 wt % PU/OMMT nanocomposites, premixed under different situations.

(e.g., from Al—OH bond) at 3626 cm^{-1} and hydrogen-bonded water bending peak at 1633 cm^{-1} [38] are of interest as both structural —OH and water are capable of reacting with —NCO groups. Also, note that C30B exhibits —CH stretching peaks at 2945 and 2851 cm^{-1}, which correspond to hydrocarbon chains of the organic ammonium ions present in this treated clay.

The clay particles in nanocomposites produced characteristic bands associated with the stretching of Si—O (1037 cm^{-1}), (which overlapped with the peak of the C—O stretching of urethane at 1092 cm^{-1}), and Si—O—Al (522 cm^{-1}), and bending of Si—O—Si at 463 cm^{-1}, as shown in Figure 7(c–f). The free —OH band at 3626 cm^{-1} and hydrogen-bonded water bending peak at 1633 cm^{-1} in organoclay disappeared in nanocomposites, indicating that strong interactions are occurring between OH group in organoclay and P-MDI.

The hydrogen-bonded NH peak at 3352 cm^{-1}, carbonyl peaks at 1703 (hydrogen-bonded) and 1729 cm^{-1} (free), appeared in pristine PU and in composites as shown in Figure 7(b–f), indicating the presence of urethane linkages.[39] The carbonyl peaks of 3 wt % PU/OMMT composites are highlighted in Figure 8 and the ratios of area under the peaks of

TABLE I
***d*-Spacing for Organoclay and PU/Clay Nanocomposites After Various Premixing Conditions**

	Specimen	2θ (°)	d_{001} basal spacing (Å)
	Cloisite 30B powder	4.87°	18.48
3 wt % OMMT/ PU composite	2-h mechanical agitation	3.21°	27.5
	15-min sonication	2.53°	34.9
	30-min sonication	2.37°	37.26
	60-min sonication	No peak	–

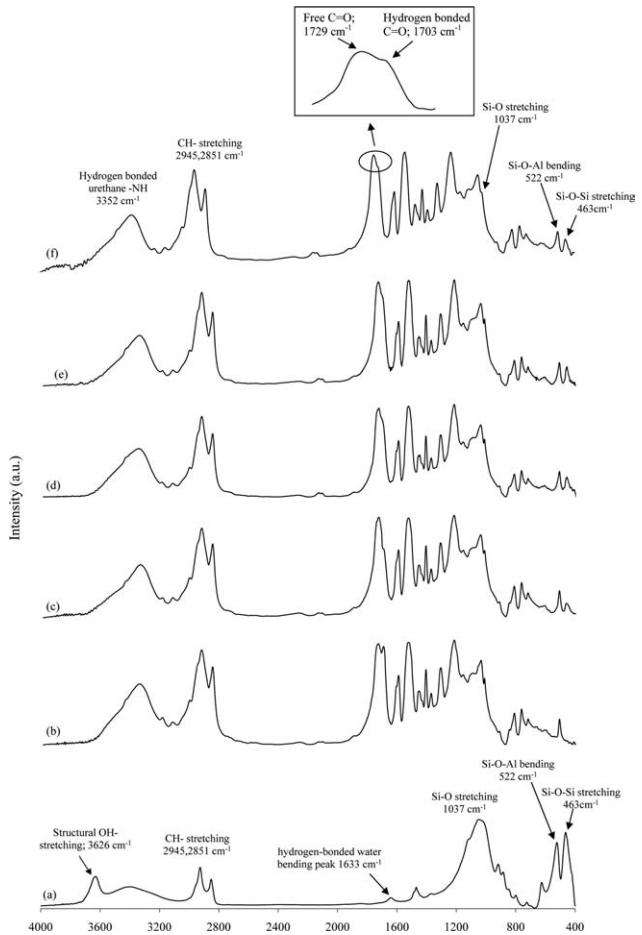

Figure 7 FTIR spectra of (a) C30B, (b) pristine PU and 3 wt % PU/OMMT composites premixed by (c) 2-h mechanical agitation, (d) 15-min sonication, (e) 30-min sonication, and (f) 60-min sonication.

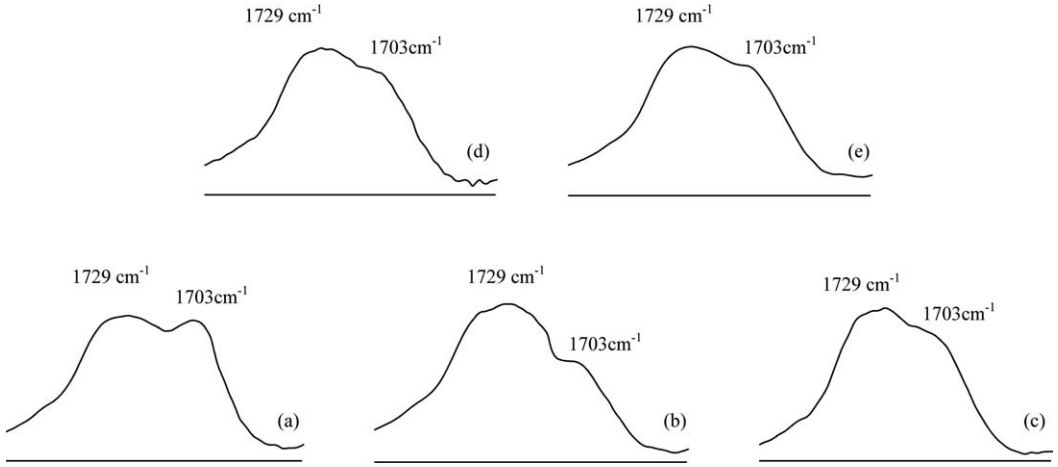

Figure 8 FTIR spectra of free (1729 cm^{-1}) and hydrogen bonded carbonyl (1703 cm^{-1}) peaks of (a) pristine PU and 3 wt % PU/OMMT composites premixed by (b) 2-h mechanical agitation, (c) 15-min sonication, (d) 30-min sonication, and (e) 60-min sonication.

hydrogen-bonded carbonyl groups at 1703 cm^{-1} (A_{HCO}) and free carbonyl groups at 1729 cm^{-1} (A_{CO}) are listed in Table II. This ratio is found to be the largest in the case of pure PU and the lowest in case of the composite prepared after 2-h mechanical agitation. This indicates that the presence of organoclay hinders the hydrogen bonding of carbonyl groups in PU matrix. However, H-bond formation is increased for composites premixed by ultrasonication process. Also, from Table II, it can be seen that increasing the ultrasonication duration from 15 to 60 min has no major effect on the hydrogen bonding of C=O group.

Improvement of the hydrogen bonding of C=O group after ultrasonication premixing step can be explained as follows. Some P-MDI chains which end with —NCO functional group can diffuse into the galleries of clay and react with CH_3CH_2OH of alkyl ammonium organifier on clay surface to form urethane linkage, which in turn tends to form hydrogen bond with the second CH_3CH_2OH group of C30B organifier as schematically illustrated in Figure 9. Another possibility is the hydrogen bond formation of C=O group of a PU chain near the clay surface with —OH group of organifier. The third possibility is the formation of H-bonding between carbonyl groups of castor oil with the clay structural or organifier —OH groups. By using sonication process which leads to improvement of interlayer spacing, the chance for aforementioned possibilities increases. The hydrogen bond formation between organifier and PU matrix leads to strong interfacial interactions between clay surface and PU and also further delamination of clay layers. Apart from the enhancement of mechanical properties, this may result in improvement in barrier properties of PU/OMMT nanocomposites.[3,8]

TABLE II
Ratio of Area Under the Peaks of Hydrogen Bonded C=O (A_{HCO}) and Free C=O (A_{FCO}) Groups Computed from Figure 8

		3 wt % PU OMMT composite			
Sample	Pristine PU	2-h mechanical agitation	15-min sonication	30-min sonication	60-min sonication
A_{HCO}/A_{FCO}	0.94	0.51	0.8	0.83	0.85

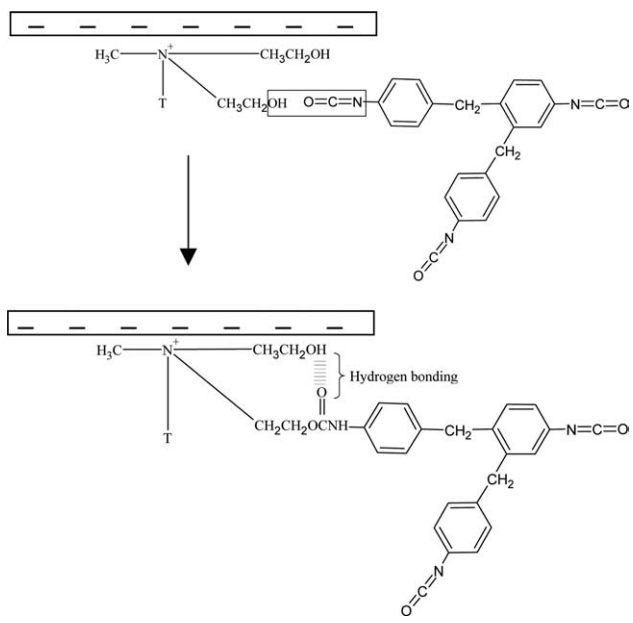

Figure 9 Hydrogen bonding between clay organifier and PU chain.

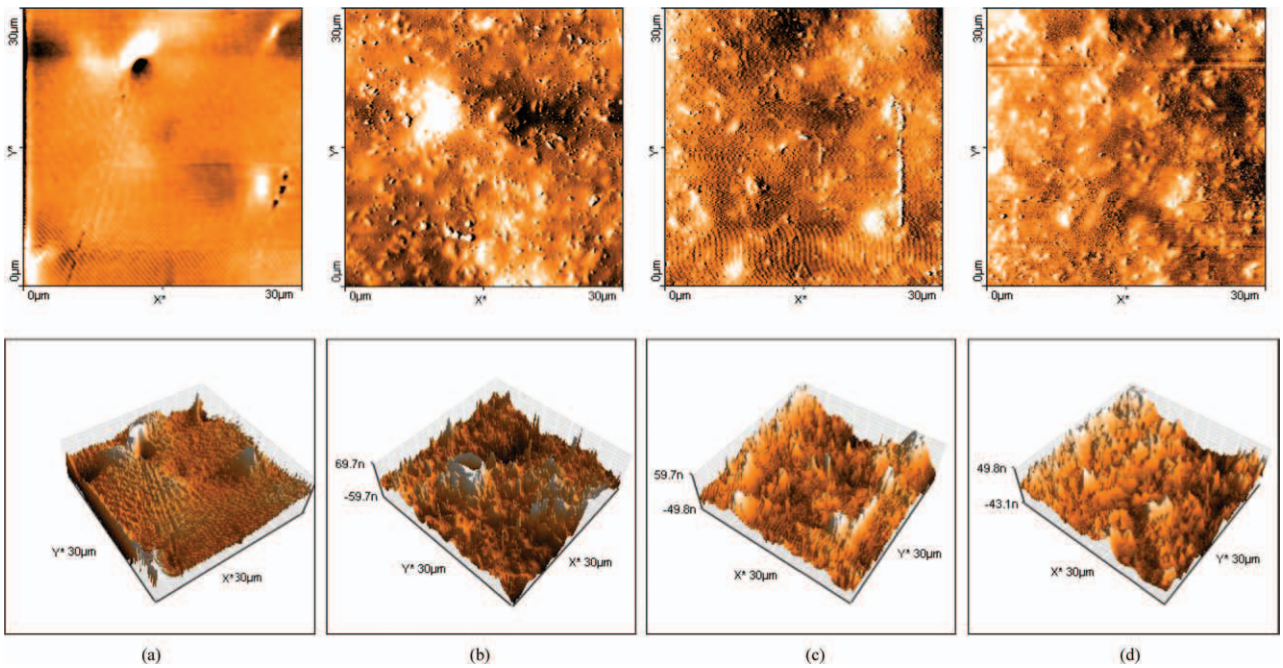

Figure 10 Typical topographic images of (a) pristine PU surface and the surfaces of 3 wt % PU/OMMT composites premixed by (b) 15-min sonication, (c) 30-min sonication, and (d) 60-min sonication. [Color figure can be viewed in the online issue, which is available at wileyonlinelibrary.com.]

Surface morphology

The topographic morphology of surface of molded specimens was scanned by AFM. Figure 10 reveals the representative pictures. The Rms data of the surface roughness of samples are listed in Table III. The AFM image of the pure PU [Fig. 10(a)] shows an extremely uniform and flat surface. The average surface roughness was around 4.87 nm. Surface morphology of nanocomposites prepared through ultrasonication assisted process is shown in Figure 10(b–d). In comparison to neat PU, the surface structure becomes irregular and average surface roughness increases by introduction of clay stacks. It confirms that nanoclay platelets seem to have influence on the surface morphology of PU films and tend to migrate toward PU surface. Also, according to Table III, it is obvious that the surface roughness decrease by increasing the sonication time up to 60 min. This may be resulted from reduction in the size of clay stacks due to extending the sonication period.

TABLE III
The Rms Values of Surface Roughness of Pure PU and Composite Films

		3 wt % PU OMMT composite		
Sample	Pristine PU	15-min sonication	30-min sonication	60-min sonication
Surface roughness (nm)	4.87	17.69	14.25	12.13

Water permeation

The influence of clay additives on permeability of a nanocomposite is depends on three main factors that are the volume fraction of the nanoplatelets, their orientation relative to the diffusion direction, and their aspect ratio. Clay layers are similar to aligned impermeable flakes, acting as barriers, increasing tortuosity of the diffusion path and decreasing permeation through the polymeric membranes. Extent of tortuosity is a function of clay content and degree of exfoliation. Therefore, to determine how the processing condition of a hybrid composite would affect the sorption and diffusion of the nanocomposites, transport properties were investigated for all prepared samples.

Figure 11 presents the water uptake profiles of pure PU and 3 wt % PU/OMMT composites after 2-h mechanical agitation and 15-, 30-, and 60-min sonication. The sorption coefficient, diffusion coefficients and permeability of samples after exposure for 2800 h were calculated and are listed in Table IV. As presented in Table IV, in the case of the composite film, prepared by 2-h mechanical agitation, sorption coefficient, and diffusivity coefficient were increased compared to that of pure PU. As was found from the results of the WAXD, mechanical agitation is not an effective method for dispersion of clay

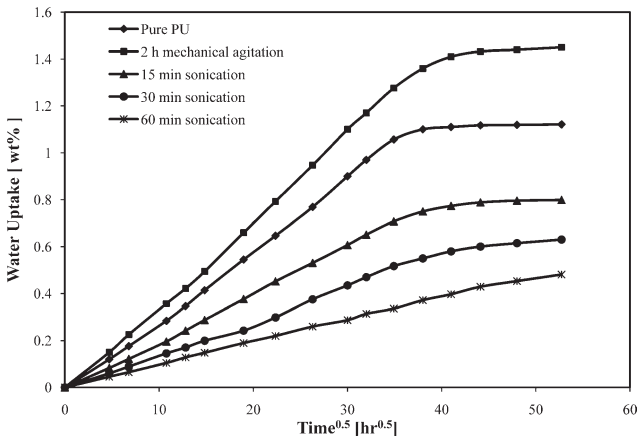

Figure 11 Water absorption curves for pure PU and nanocomposite films after certain time intervals.

agglomerates and delamination of clay layers. Therefore, poor dispersion of nanoparticles leads to inferior barrier property. This is probably due to gathering of water molecules around the clay particles, which are poorly bonded to PU matrix, and also at the mechanically weak spots around the regions of clay agglomeration.[40]

However, as is clearly presented in Figure 11 and Table IV, the sorption coefficient and diffusivity coefficient is decreased by using sonication process and increasing its duration to 60 min, when compared with neat PU. Also, in the case of nanocomposite specimen, prepared by 60-min sonication premixing, the full saturation is not reached even after 2800 h.

As previously mentioned, the water sorption behavior is considered as dependent on free volume (free water trapped in microvoids of free volume) properties and type and concentration of hydrophilic groups in the PU system.[41] As discussed before, increasing sonication duration results in better dispersion and reduction in particle size of clay agglomerates, along with higher aspect ratio of the clay particles which in turn leads to higher interfacial interactions between clay surface and PU matrix. These in turn increase the tortuosity of the pathway of water molecules as diffused into the nanocomposites and also decrease the free volume in pure PU for water accumulation. Also, the decreased sorption coefficient, diffusivity coefficient and therefore permeability are related to the presence of strong interactions and hydrogen bonding formations between PU and modifier on clay platelets, and hydrogen bonding interactions in the composites tend to stabilize the nanocomposites when subjected to highly moist atmosphere. As a result, the maximum water uptake and diffusivity of nanocomposites were decreased, compared with pure PU.

Electrochemical impedance spectroscopy

To study the barrier properties of 3 wt % PU/OMMT composites, prepared by different processing conditions and to evaluate the corrosion performance of these composites as protective organic coatings on carbon steel panels, EIS was performed. Figures 12–14 show the Bode plots of the coated panels during 21 days of immersion in 5 wt % NaCl aqueous solution. As is clear from the figures, all the coated panels show only one capacitive time constant until 21 days of exposure (Figs. 12–14). Such an electrochemical behavior can be described in terms of simple equivalent circuit depicted in Figure 15(a), which consists of the parallel combination of a dielectric capacitor C_C (coating capacitance) and a resistive component R_C (coating resistance). Analysis of the impedance spectra in terms of this equivalent circuit allowed for the parameters R_C and C_C to be determined. Changes in the magnitudes of these parameters, as a function of their exposure time to the test solution, are plotted in Figure 16(a,b). As shown in Figure 16, C_C increases with the immersion time due to water uptake (Because of the much higher dielectric constant of water compared with that of organic coating), whereas R_C decreases with time (Because of the much lower resistivity of water compared to that of organic coating and development of ionic conductive pathways in polymer).

As illustrated in Figure 12, it is obvious that all PU/OMMT composite-coated panels have higher

TABLE IV
Equilibrium Water Uptake and Diffusion Coefficient of Pure PU and 3 wt % OMMT/PU Composite Films Prepared Through Different Premixing Conditions

	Sample	Sorption	Diffusivity (10^{-7} mm^2 sec^{-1})	Permeability (10^{-9} mm^2 sec^{-1})
	Pristine PU	0.01121	2.98	3.3406
3 wt % OMMT/PU composite	2-h mechanical agitation	0.0145	3.09	4.4805
	15-min sonication	0.0081	2.79	2.2599
	30-min sonication	0.0063	2.56	1.6128
	60-min sonication	0.0049	2.23	1.0927

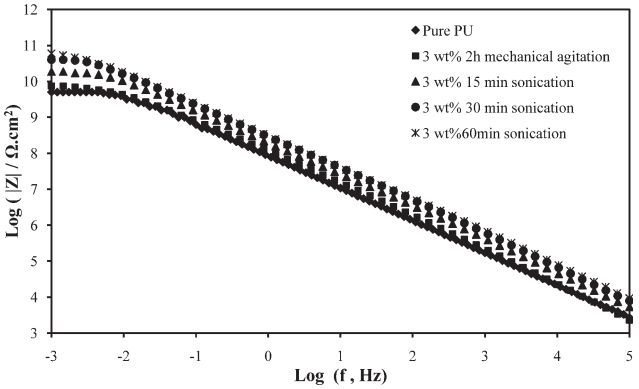

Figure 12 Representative Bode diagrams of neat PU and 3 wt % PU/OMMT composite coated panels (prepared through different premixing conditions) before immersion.

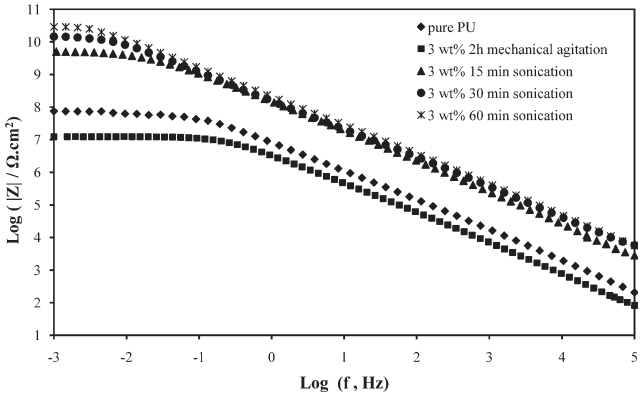

Figure 14 Representative Bode diagrams of neat PU and 3 wt % PU/OMMT composite coated panels (prepared through different premixing conditions) after 21 days immersion.

impedance values than pure PU before exposure to corrosive media. By exposing the coated panels to the test solution, it can be seen that in the case of samples prepared through the ultrasonication-assisted process, the values of R_C were still higher at different immersion times than pure PU, and the 60-min sonicated specimen showed the highest R_C values [Fig. 16(a)]. Also, it is found that the reduction in R_C values during immersion is decreased as the sonication duration in premixing step is increased. These findings are in good agreement with the results of water permeation test. As discussed earlier, increasing the sonication duration improves dispersion and aspect ratio of clay particles which effectively increase the length of the diffusion pathways for oxygen and water and decrease the permeability of the coating. However, in the case of 3 wt % PU/OMMT composite system, prepared after 2-h mechanical agitation, the R_C values are lower in comparison with pure PU after various exposure durations. As it was discussed above, this is due to poor dispersion of clay stacks in PU matrix.

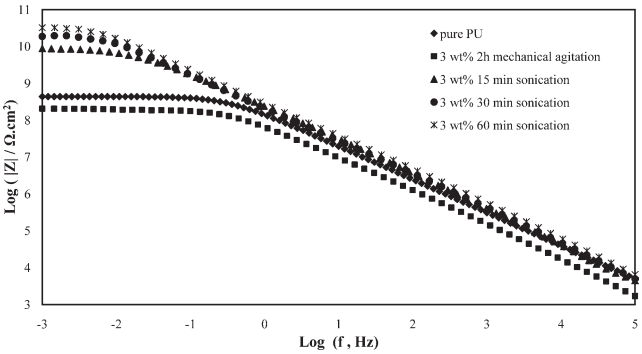

Figure 13 Representative Bode diagrams of neat PU and 3 wt % PU/OMMT composite coated panels (prepared through different premixing conditions) after 13 days immersion.

The volumetric water uptake values obtained from eq. (7) are shown in Table V for 30 days under immersion of the coated samples. These results show a trend, similar to that obtained in water permeation test. The lowest value of water uptake is related to 60 min sonicated nanocomposite-coated panel and the highest is related to 2 h mechanically agitated one.

As presented in Figure 17, the Bode plots of pure PU and 2 h mechanically agitated coated panels are

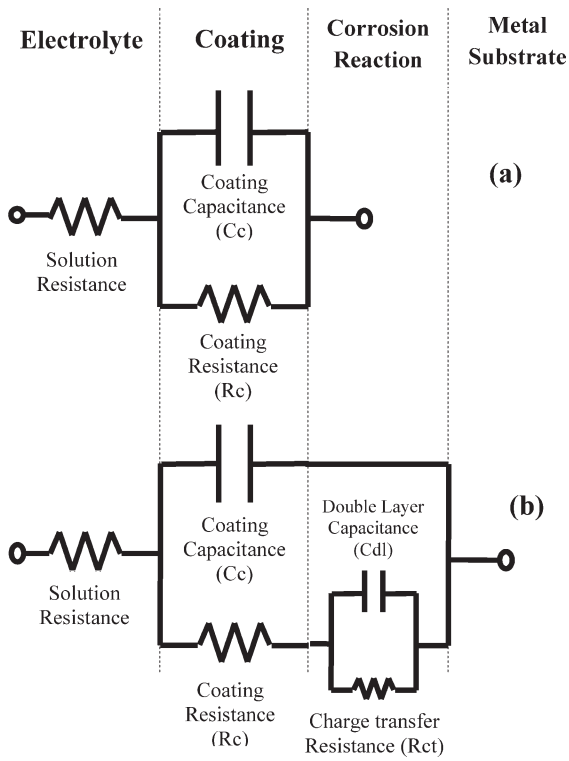

Figure 15 Equivalent circuits for the description of (a) barrier coating system with one time constant and (b) non-barrier coating system with two time constants.

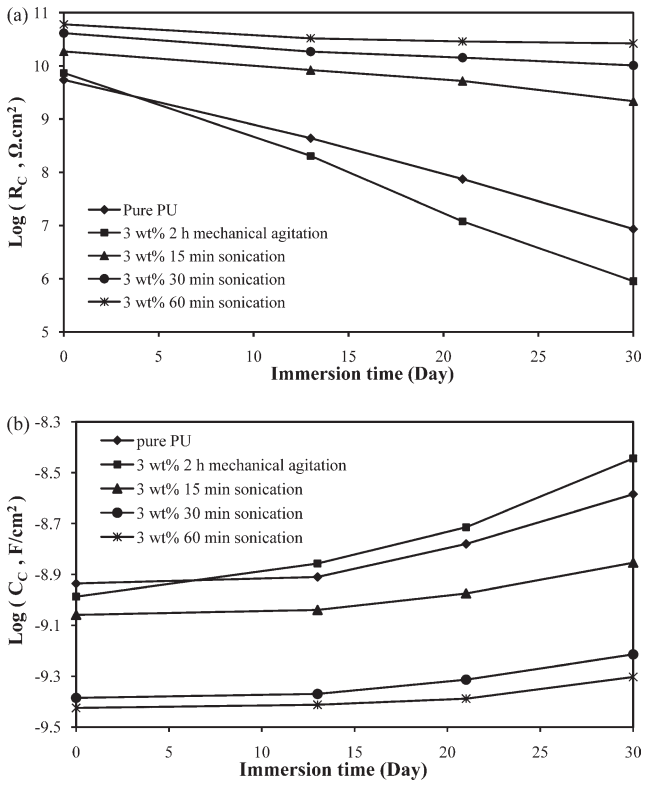

Figure 16 (a) R_C and (b) C_C versus immersion time in 5 wt % NaCl solution for neat PU and 3 wt % PU/OMMT composite coated specimens, prepared through different premixing conditions.

split into two sections, which indicate the development of second time constant in the impedance diagrams of these two samples after 30 days under immersion (one at high frequencies, corresponding to coating parameters, and one at low frequencies, corresponding to electrochemical corrosion reaction on the substrate). Under this condition, the equivalent circuit which adequately describes the measured impedance spectra for a defective organic-coated metal is given in Figure 15(b). In this model, the new components are a capacitor C_{dl} (double layer capacitance), which accounts for the distribution of ionic charges around the unprotected metallic substrate and a new resistive element, R_{ct} (charge transfer resistance), which is inversely proportional to the corrosion rate of the metal.[42] This indicates that these panels are no longer effectively protected against corrosion, and, therefore, the corrosion attack at the metal/coating interface has already initiated. However, even after 30 days under immersion, in the case of the panels coated with nanocomposites prepared through the ultrasonication-assisted premixing step, only one capacitive time constant could be detected in EIS spectra. This shows that the corrosion process has not been initiated on substrate, and the nanocomposite coatings still prevent the underlying metal to come in direct contact with the aqueous environment.

CONCLUSIONS

In this study, a series of 3 wt % PU/OMMT nanocomposites were synthesized under different processing conditions through *in situ* polymerization method by using mechanical agitation and various durations of sonication process. Results of optical microscopy, sedimentation test, and viscosity measurement indicate that by application of sonication process and increasing its duration, the size of clay agglomerates is decreased and their number per unit volume is increased, which result in formation of viscous stable suspensions of castor oil/OMMT. WAXD analysis showed improvement in interlayer spacing by increasing sonication time. Form the FTIR results, it is found that by using sonication process, the H-bonding formation between clay layers and PU matrix is increased, compared with the composite specimen which processed only by mechanical agitation. Also, AFM revealed that surface roughness is increased by introduction of OMMT in comparison with neat PU. However, as the sonication duration is increased, the surface roughness is decreased. Calculation of diffusion coefficient and maximum water uptake revealed that the PU/OMMT composite specimen, which premixed by mechanical agitation, had inferior barrier properties than pure PU, resulted from the poor dispersion of clay layers in PU matrix. However, by application of sonication process and increasing the processing duration, an improvement in transport properties against diffusion of water molecules was observed.

TABLE V
The Percentage of Water Taken Up by Volume (X_v), Calculated From Composite Capacitance at Various Exposure Times as Shown in Figure 16(b)

		3 wt % OMMT/PU Composite			
Days of immersion	Pristine PU	2-h mechanical agitation	15-min sonication	30-min sonication	60-min sonication
13 days	1.33	6.84	1.02	0.81	0.65
21 days	8.17	14.33	4.49	3.7	1.92
30 days	18.42	28.02	10.78	8.97	6.41

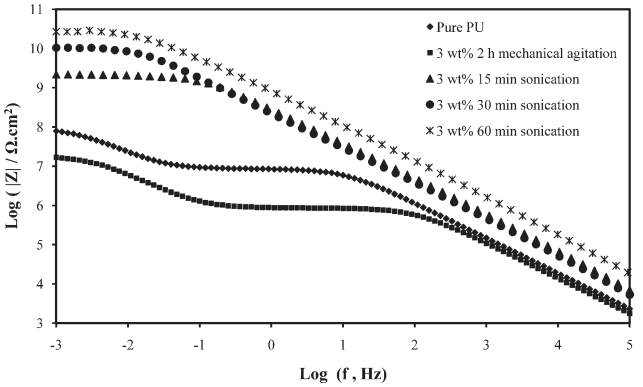

Figure 17 Representative Bode diagrams of neat PU and 3 wt % PU/OMMT composite coated panels (prepared through different premixing conditions) after 30 days immersion.

These findings were confirmed by EIS. Also, from EIS results, it was found that in the case of carbon steel panels, coated with neat PU and the composite specimen, which premixed by only mechanical agitation, the corrosion process has initiated on metallic substrate after 30 days immersion. This is due to lack of ability of these two systems to prevent diffusion of oxygen and water molecules, which results in direct contact of corrosive species with metal substrate. However, in case of the panels, coated by sonicated PU/OMMT nanocomposites, no sign of corrosion attack was observed and coating resistance (R_C) was increased by increasing sonication time. This is due to better dispersion and delamination of clay layers, which effectively increases the length of the diffusion pathways for oxygen and water.

The authors thank Dr. A. Ashrafi, Mr. M. Sadeqzadeh, and Dr. D. Zaarei for helpful suggestions and comments.

References

1. Bagherzadeh, M. R.; Mahdavi, F. Prog Org Coat 2007, 60, 117.
2. Heidarian, M.; Shishesaz, M. R.; Kassiriha, S. M.; Nematollahi, M. Prog Org Coat 2010, 68, 180.
3. Bongiovanni, R. E.; Turcato, A.; Gianni, A. D.; Ronchetti, S. Prog Org Coat 2008, 62, 336.
4. Sangermano, M.; Lak, N.; Malucelli, G.; Samakande, A.; Sanderson, R. D. Prog Org Coat 2008, 61, 89.
5. Ahmadi, B.; Kassiriha, S. M.; Khodabakhshi, K.; Mafi, E. R. Prog Org Coat 2007, 60, 99.
6. Choi, H. Y.; Bae, C. Y.; Kim, B. K. Prog Org Coat 2010, 68, 356.
7. Qunhui, S. F.; Joseph, S.; Yulin, D. Compos Sci Technol 2007, 67, 1823.
8. Jia, Q. X.; Wu, Y. P.; Wang, Y. Q.; Lu, M.; Zhang, L. Q. Compos Sci Technol 2008, 68, 1050.
9. Esposito, C.; Prinari, P.; Cannoletta, D.; Mensitierib, G.; Maffezzoli, A. Int J Adhes Adhes 2008, 28, 91.
10. Raka, L.; Bogoeva-Gaceva, G.; Lu, K.; Loos, J. Polymer 2009, 50, 3739.
11. Giannakas, A.; Spanos, C. G.; Kourkoumelis, N.; Vaimakis, T.; Ladavos, A. Eur Polym Mater 2008, 44, 3915.
12. Ray, S. S.; Okamoto, M. Prog Polym Sci 2003, 28, 1539.
13. Daud, W.; Bersee, H.; Picken, J. S.; Beukers, A. Compos Sci Technol 2009, 69, 2285.
14. Ray, S. S.; Bousmina, M. Prog Mater Sci 2005, 50, 962.
15. Herrera-Alonso, J. M.; Marand, E.; Little, J.; Cox, S. S. Polymer 2009, 50, 5744.
16. Kim, J. K.; Hu, C.; Woo, R.; Sham, M. L. Compos Sci Technol 2005, 65, 805.
17. Liu, W.; Hoa, S. V.; Pugh, M. Compos Sci Technol 2007, 67, 3308.
18. Uddin, M. F.; Sun, C. T. Compos Sci Technol 2010, 70, 223.
19. Ratinac, K. R.; Gilbert, R. G.; Ye, L.; Jones, A. S.; Ringer, S. P. Polymer 2006, 47, 6337.
20. Rangari, V. K.; Hassan, T. A.; Mayo, Q.; Jeelani, S. Compos Sci Technol 2009, 69, 2293.
21. Paul, D. R.; Robeson, L. M. Polymer 2008, 49, 3187.
22. Ngo, T. D.; Ton-That, M. T.; Hoa, S. V.; Cole, K. C. Compos Sci Technol 2009, 69, 1831.
23. Pavlidou, S.; Papaspyrides, C. D. Prog Polym Sci 2008, 33, 1119.
24. Herrera-Alonso, J. M.; Marand, E.; Little, J. C.; Cox, S. S. J Membr Sci 2009, 337, 208.
25. Liu, W.; Hoa, S. V.; Pugh, M. Compos Sci Technol 2005, 65, 2364.
26. Lam, C.; Lau, K.; Cheung, H.; Ling, H. Mat Lett 2005, 59, 1369.
27. Wang, J; Qin, S. Mat Lett 2007, 61, 4222.
28. Chen, Y.; Zhou, S.; Yang, H.; Gu, G.; Wu, L. J Colloid Interface Sci 2004, 279, 370.
29. Moly, K. A.; Bhagawan, S. S.; George, S. C.; Thomas, S. J Mater Sci 2007, 42, 4552.
30. Johnson, T.; Thomas, S. J Mater Sci 1999, 34, 3221.
31. Hinderliter, B. R.; Allahar, K. N.; Bierwagen, G. P.; Tallman, D. E.; Croll, S. G. J Coat Technol Res 2008, 5, 431.
32. Rezaei, F.; Sharif, F.; Sarabi, A. A.; Kasiriha, S. M.; Rahmanian, M.; Akbarinezhad, E. J Coat Technol Res 2010, 7, 209.
33. Rammelt, U.; Reinhard, G. Prog Org Coat 1992, 21, 205.
34. Zhaoa, J.; Morganb, A. B.; Harris, J. D. Polymer 2005, 46, 8641.
35. Labruyère, C.; Gorrasi, G.; Monteverde, F.; Alexandre, M.; Dubois, P. Polymer 2009, 50, 3626.
36. Liu, W.; Hoa, S. V.; Pugh, M. Compos Sci Technol 2008, 68, 2066.
37. Lin-Gibson, S.; Kim, H.; Schmidt, G.; Han, C. C.; Hobbie, E. K. J Colloid Interface Sci 2004, 274, 515.
38. Pattanayak, A.; Jana, S. C. Polymer 2005, 46, 3275.
39. Rehab, A.; Salahuddin, N. Mater Sci Eng A 2005, 399, 368.
40. Becker, O.; Varley, R. J.; Simon, G. P. Eur Polym Mater 2004, 40, 187.
41. Jia, Q. M.; Zheng, M.; Chen, H. X.; Shen, R. J Polym Bull 2005, 54, 65.
42. Macedo, M. C. S. S.; Margarit-Mattos, I. C. P. F. L.; Fragata, J. B.; Jorcin, N. P.; Mattos, O. R. Corros Sci 2009, 51, 1322.